Current Source Inverter Based Large Constant Power Speed Ratio SPM Machine Drive for Traction Applications

Feida Chen, Hao Ding, Sangwhee Lee, Wenda Feng, Thomas M. Jahns, Bulent Sarlioglu
Wisconsin Electric Machines and Power Electronics Consortium (WEMPEC)
University of Wisconsin-Madison, WI 53706 USA
E-mail: *sarlioglu@ wisc.edu*

Abstract- **A high-performance surface permanent magnet (SPM) machine drive with an extended constant power speed ratio is proposed using a current source inverter (CSI) for a traction application. The constant-power operation regions of an SPM machine can be extended in an appealing fashion by taking advantage of the output voltage boost capability of the CSI. The CSI is naturally a boost-type converter, in contrast to the voltage source inverter (VSI) which has buck-type characteristics. To investigate the value of the CSI voltage boost feature, a new traction motor with higher rated voltage and lower rated current has been designed and compared to the motor that would be used with a VSI. The lower CSI current makes it possible to reduce the mass of the inverter and output power cable, benefiting power density and cost reduction. The SPM machine is modeled in the synchronous reference frame including the effect of the ac filter capacitors at the CSI output terminals. The capability of extending the speed range of the proposed motor is verified via closed-form analysis and FEA simulation, and its performance characteristics are compared with those of a VSI-based SPM motor of the same type.**

Keywords **– current source inverter, SPM machine, voltage boost, wide speed range, traction application**

I. Introduction

Due to the global energy crisis and environmental pollution, electric vehicles (EVs) have been aggressively developed around the world during the past decade [1,2]. The surface permanent magnet (SPM) machine offers advantages for EV applications due to their appealing features including high torque density, high overload capability, and convenient controllability characteristics [3]. In addition, the SPM machine can achieve excellent flux weakening characteristics by using fractional-slot concentrated windings. Some types of EVs such as trucks and off-road construction vehicles, benefit from high constant-power speed ratio (CPSR) values that can reach values of 10 or higher in some cases [4]. However, requirements for such deep flux weakening operation can pose problems for conventional VSI-based traction drives because the output voltage is limited by the dc-bus voltage [5] which equals the battery voltage in many cases. In contrast, the CSI operates naturally as a boost-type inverter that can raise the motor terminal voltage above the dc-link voltage, offering advantages for achieving high CPSR values with reduced inverter and motor current ratings.

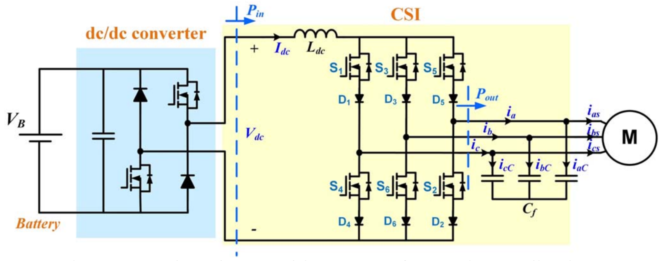

Fig. 1. CSI based motor drive system for traction application

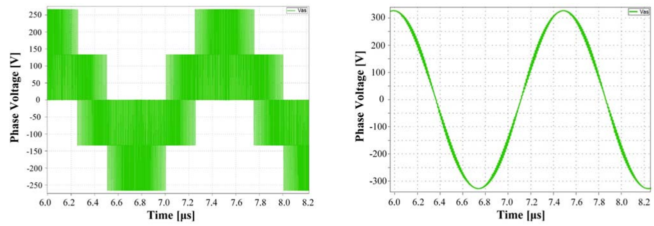

Fig. 2. Simulated output line-to-netrual voltage of VSI (left) and CSI (right)

A CSI-based traction drive configuration is shown in Fig. 1 [6]. Adoption of wide band-gap (WBG) switches in the CSI makes it possible to operate the CSI at very high switching frequencies which, in turn, offers several drive system advantages. The WBG-based CSI replaces the thermally-limited dc-link capacitor (< 150 ºC) in the VSI with a compact high-temperature inductor (> 200 ºC), improving the high-temperature compatibility of the inverter. The three small ac capacitors connected to the output terminals of CSI function naturally as a low-pass filter in combination with the dc bus inductors, resulting in much more sinusoidal output voltage waveforms, as shown in Fig. 2, and lower common-mode EMI emissions compared to the VSI [7].

In the 1980s, a GTO-based CSI was investigated for an induction motor drive application [8,9], but the GTO's low switching frequency created limitations for this approach. As silicon MOS-gated switches were commercialized during the 1980s, CSIs lost their competition with VSIs for motor drive applications because of the natural suitability of the MOS-gated devices to VSI applications [10]. However, the recent emergence of wide-bandgap power devices opens opportunities for the long-ignored CSI to provide a promising alternative drive configuration for traction applications. Dai, *et al* [7,11] demonstrated that the CSI offers valuable performance advantages over VSI when WBG power switches are introduced. Su, *et al* [6,12] investigated the value of the boost feature of CSIs to extend the constant-power speed range for EV applications. Nevertheless, little attention has been focused on machine designs specifically tailored to take full advantage of this special CSI feature. During this study, a new SPM machine has been specially designed to fully utilize the voltage boost capability of CSI to extend the speed range.

This paper investigates the CSI voltage boost function and proposes a CSI-based SPM machine with higher voltage and lower current ratings. Using this approach, a large CPSR can be successfully achieved in combination with the CSI. In Section II, the voltage-boosting feature of the CSI is investigated. In Section III, the SPM machine is modeled including consideration of the CSI's ac capacitors. Section IV discusses the proposed SPM machine design which is optimized for the CSI. In Section V, the capability of extending the speed range of the proposed motor is verified using FEA simulations and compared with the corresponding characteristics with a VSI-based motor. The conclusions are discussed in Section V.

II. Voltage Boost Function of CSI

A notable advantage of the CSI over a conventional VSI in traction drive applications is the CSI's natural output voltage boost function [12]. When the two switches in a single phase leg of a CSI are turned on at the same time, no output terminal current flows either to the filter capacitors or the motor load. Instead, this condition creates a short-circuit state (zero vector) that charges the dc-link inductor and increases the inductor current. After the CSI switches to an active current state, the inductor current charges (or discharges) the capacitors and varies the instantaneous output voltage applied to the machine, changing its phase current in the process. As a result of this behavior, the CSI operates as a boost converter. The relationship between the boost ratio and the modulation index of CSI can be described in (1)-(3).

$$P_{in} = V_{dc} \cdot I_{dc} \tag{1}$$

$$P_{out} = 3V_{pk}I_{pk}cos(\theta + \varphi)/2 \tag{2}$$

where P_{in} and P_{out} are the instantaneous input power and output power of the CSI, respectively, measured at the terminals of the ac capacitors at the CSI power stage output; V_{dc} and I_{dc} are the average dc-link voltage and current, respectively, at the input terminals of the dc-link inductor; V_{pk} and I_{pk} are the peak line-to-neutral voltage and phase current that excites the wye-connected three-phase load, θ is the angle between the motor phase voltage and phase current (i.e., power factor angle), and φ is the angle between the CSI output current and motor phase current.

Assume there are no power losses in the CSI, so that $P_{in} = P_{out}$. The voltage boost ratio can then be derived from (1)-(3) to be:

$$\frac{V_{pk}}{V_{dc}} = \frac{2}{3cos(\theta + \varphi)} \cdot \frac{1}{m} \tag{3}$$

where m is the scalar modulation index of the CSI, defined as:

$$m = \frac{I_{pk}}{I_{dc}} \tag{4}$$

It is apparent from equation (3) that the boost ratio increases as the magnitude of the modulation index of CSI decreases.

This voltage-boosting feature of the CSI offers multiple advantages for traction drive applications: (a) When the battery voltage drops, the CSI can boost the output voltage to maintain the same output power, while the VSI needs a front-end boost converter to provide this same desirable feature; and (b) The voltage boost function of the CSI can be used to improve the machine's constant-power operating characteristics to achieve a high CPSR at a higher output power value even when V_{dc} decreases.

III. SPM Machine Model Considering AC Capacitor Effect

The three small ac capacitors connected to the CSI's output terminals are necessary for CSI operation. These capacitors naturally function as a low-pass filter in combination with the dc bus inductor, resulting in much more sinusoidal output voltage waveforms and lower common-mode EMI compared to a VSI. The capacitors behave as current-controlled voltage sources that cannot be ignored in the high-speed region. Thus, the *d-q* equivalent circuits of an SPM machine in the rotor reference frame incorporating the effect of the ac capacitors to reduce modeling error are provided in Fig. 3 [13].

The simplified SPM machine model in the rotor reference frame can be represented by the following equations.

$$v_{qs} = r_s i_{qs} + \omega_e L_d i_{ds} + \omega_e \lambda_m + L_q p i_{qs} \tag{5}$$

$$v_{ds} = r_s i_{ds} - \omega_e L_q i_{qs} + L_d p i_{ds} \tag{6}$$

where v_{qs} and v_{ds}, i_{qs} and i_{ds}, L_q and L_d are the *q*- and *d*- axis voltage, current, and inductance of SPM machine, respectively; r_s is the stator resistance; ω_e is the motor electrical speed; and λ_m is the flux linkage. Also, a derivative operation p is used to simplify the (5) and (6) expressions.

For steady-state operating conditions, the *q*- and *d*-axis voltages and currents of the motor can be related by

$$v_{qs} = r_s i_{qs} + \omega_e L_d i_{ds} + \omega_e \lambda_m \tag{7}$$

$$v_{ds} = r_s i_{ds} - \omega_e L_q i_{qs} \tag{8}$$

Considering the ac capacitor effect, the vector diagram of the CSI-based motor in the rotor reference frame is shown in Fig. 4. It should be noted that the rotor and synchronous reference frames are identical, but only for steady-state operating conditions.

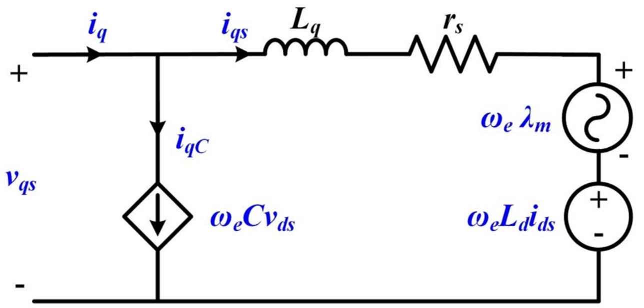

(a) q-axis equivalent circuit

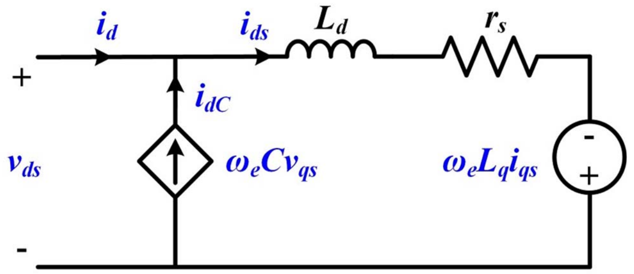

(b) d-axis equivalent circuit

Fig. 3. d-q equivalent circuits of the SPM motor considering ac capacitors

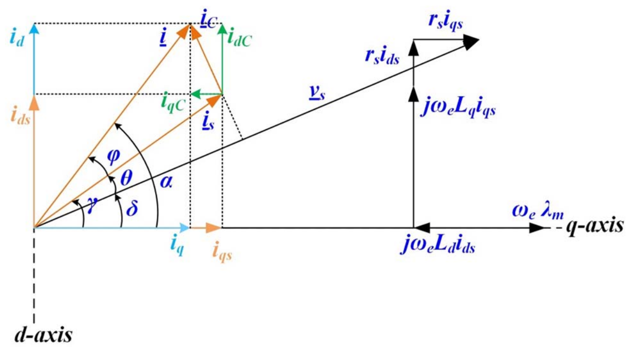

Fig. 4. Vector diagram of the CSI-based motor

In Fig. 4, α is the angle between the back-EMF of the motor and CSI output current which is the current before the capacitors; θ is the angle between output phase voltage and stator phase current (the current after the capacitors), which is power factor angle of the machine; γ is the angle between back-EMF and stator current, which is the internal power factor angle (also known as the current angle); δ is the angle between output phase voltage and back-EMF (known as the torque or load angle), and φ is the angle between CSI output current and stator current.

The steady-state q- and d- axis currents of CSI (before the capacitors) can be expressed as:

$$i_q = i_{qs} + \omega_e C v_{ds} \tag{9}$$

$$i_d = i_{ds} - \omega_e C v_{qs} \tag{10}$$

The relationship between the CSI output currents and motor voltages during steady-state operation can be calculated from (7), (8), (9) and (10) as

$$v_{qs} = r_s \frac{d \cdot i_q - a \cdot i_d + a \cdot e}{b \cdot d - a \cdot c} + \omega_e L_d \frac{c \cdot i_q - b \cdot i_d + b \cdot e}{a \cdot c - b \cdot d} + \omega_e \lambda_m \tag{11}$$

$$v_{ds} = r_s \frac{c \cdot i_q - b \cdot i_d + b \cdot e}{a \cdot c - b \cdot d} - \omega_e L_q \frac{d \cdot i_q - a \cdot i_d + a \cdot e}{b \cdot d - a \cdot c} \tag{12}$$

where $a = \omega_e C r_s$,
$b = (1 - \omega_e{}^2 C L_q)$,
$c = \omega_e C r_s i_{qs}$,
$d = (1 - \omega_e{}^2 C L_d)$,
$e = (-\omega_e{}^2 C \lambda_m)$.

The steady-state CSI q- and d-axis output currents can be controlled directly by the modulation index as:

$$i_q = I_{dc} \cdot m \cdot cos\alpha \tag{13}$$

$$i_d = I_{dc} \cdot m \cdot sin\alpha \tag{14}$$

In the constant-torque region, the CSI current angle α can be directly controlled to produce $i_{ds} = 0$, which will yield maximum torque per ampere (MTPA) control for an SPM machine. In the constant-power region, the CSI current angle α, as shown in Fig. 4, is regulated to generate a flux-weakening component $i_{ds} < 0$. In addition, the magnitude of the modulation index m of CSI can be controlled to boost the machine terminal voltage, as mentioned above, in order to increase the corner-point speed of the machine (i.e., the transition speed from constant-torque to constant-power operation) and raise its output power [6].

IV. SPM MACHINE DESIGN FOR CSI

For the VSI-based motor, the peak line-to-neutral voltage is bounded by the voltage limit of the VSI when using a space vector pulse width modulation (SVPWM) algorithm, which is given as

$$V_{pk(VSI)} = \frac{\sqrt{3}}{2} \cdot \frac{2}{3} V_{dc} = 0.577 V_{dc} \tag{15}$$

where $V_{pk(VSI)}$ is the peak line-to-neutral voltage of the VSI.

For VSI, assuming the battery voltage equals to 650 V, the motor terminal voltage needs to be kept below 266 Vrms line-to-neutral considering the inverter voltage capability based on (15). During flux-weakening operation, VSI-based motor must apply increase amplitudes of negative d-axis current i_{ds} to satisfy the voltage limit constraint as the speed increases. In contrast, the CSI motor voltage can be higher than that of the VSI motor because the CSI operates as a voltage boost-type inverter. Using (3), the steady-state relationship between the CSI output voltage and dc-link voltage as a function of the modulation index m is expressed as:

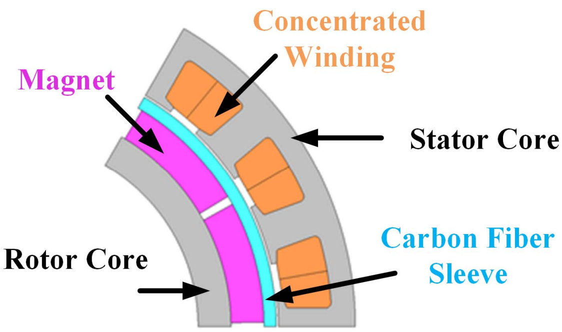

Fig. 5. Configuration of the proposed SPM machine

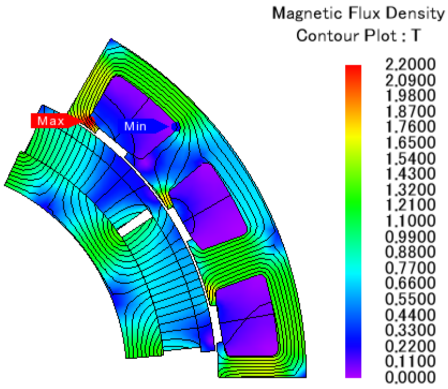

Fig. 6. Flux density distribution of the CSI-based SPM machine at rated condition

$$V_{pk(CSI)} = \frac{2}{3cos(\theta+\varphi)} \cdot \frac{1}{m} V_{dc} = \frac{0.667}{mcos(\theta+\varphi)} V_{dc} \tag{16}$$

$$V_{dc} = \frac{mV_{pk(CSI)}cos(\theta+\varphi)}{0.667} \tag{17}$$

where $V_{pk(CSI)}$ is the peak line-to-neutral voltage of the CSI.

When the magnitude of the modulation index of the CSI is maximum ($m = 1$), (16) can be simplified as

$$V_{pk(CSI)} = \frac{0.667}{cos(\theta+\varphi)} V_{dc} \tag{18}$$

It is apparent from (15) and (18) that the inherent voltage limit of the CSI is higher than the VSI even when the modulation index of the CSI equals 1. During flux-weakening operation, the product of modulation index, peak output voltage, and power factor of CSI ($m \cdot V_{pk(CSI)}cos(\theta+\varphi)$) is controlled to be constant for the CSI to maintain constant power, as reflected in (17). This relationship shows that it is convenient to raise the motor terminal voltage above the dc-link voltage by reducing the modulation index. Operating the machine at a higher terminal voltage makes it possible to reduce the negative d-axis current amplitude during flux-weakening operation. This reduction in i_{ds} means that more of the available CSI output current can be allocated to i_{qs}, raising the SPM machine's output torque and, thus, its output power. The net effect is to raise the corner-point speed of the machine ω_{cp} and the maximum deliverable power above that transition-point speed.

Because of the different voltage limits, two SPM machines with the same geometry and electrical loading but with the different number of winding turns have been configured for the CSI and VSI. The parameters of the proposed SPM machine are shown in TABLE I.

TABLE I: SPM MACHINE CONFIGURED FOR CSI AND VSI

Parameter	CSI Motor	VSI Motor
Corner speed [rpm]	3,200	
Max speed [rpm]	20,000	
Stator/rotor material	10JNHF600	
Permanent magnets	N38 NdFeB	
Number of stator slots	18	
Number of rotor poles	12	
Current density [A_{rms}/mm^2]	20	
Number of turns per coil	102	66
d-axis inductance [mH]	0.973	0.49
q-axis inductance [mH]	0.984	0.5
Phase winding resistance [Ω]	0.142	0.071
Line-to-neutral back-EMF @ 3,200 rpm [V_{rms}]	301.5	212.8
No-load flux linkage λ_m [Wb_{rms}]	0.15	0.106
Characteristic current = λ_m/L_d [A_{rms}]	154.2	216
Rated line-to-neutral voltage @ peak power [V_{rms}]	378.3	266
Rated phase current @ peak power [A_{rms}]	123.3	174.7
Rated torque @ peak power [Nm]	301	301
Continuous output power rating [kW]	55.9	55.7
Peak output power rating [kW]	100.8	100.8

Both machines are designed to deliver 100 kW peak output power at the same corner speed of 3,200 rpm, and the maximum speed is 20,000 rpm for both machines. A cross-section view of the proposed SPM machine used for both inverter types is shown in Fig. 5. A carbon fiber composite sleeve is used to retain the magnets, especially at high-speed conditions. Concentrated windings have been adopted to lower the machine's characteristic current value sufficiently to achieve high CPSR values as well as to limit the axial length by shortening the winding end turns.

A 12-pole topology was selected to limit the fundamental frequency to 2,000 Hz at the maximum speed of 20,000 rpm. A segmented stator configuration with 18 slots was selected using 6 parallel windings to minimize the inverter bus voltage for the desired output power.

The flux density distribution of the CSI-based SPM machine at the rated output power condition is shown in Fig. 6. The peak flux density in the airgap is approx. 1.2 T and the maximum lamination flux density (saturated) is 2.02 T in the stator tooth

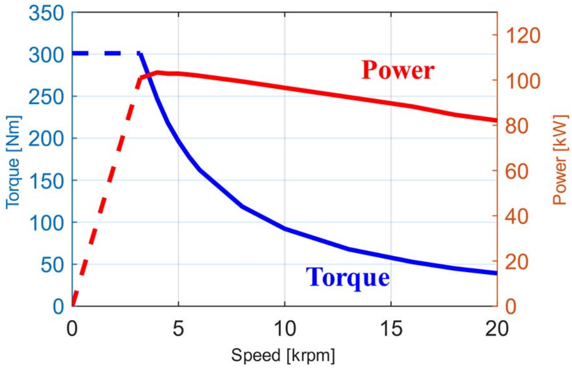

Fig. 7. FEA-based torque vs. speed and power vs. speed envelope curves of CSI motor drive

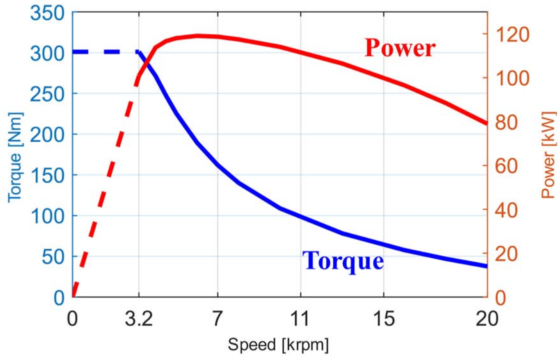

Fig. 8. FEA-based torque vs. speed and power vs. speed envelope curves of VSI motor drive

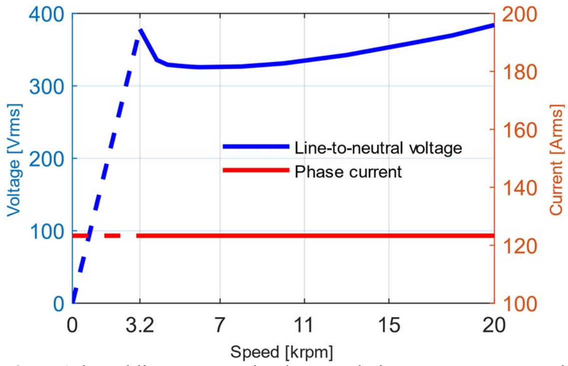

Fig. 9. FEA-based line-to-neutral voltage and phase current vs. speed envelope curves of CSI motor drive

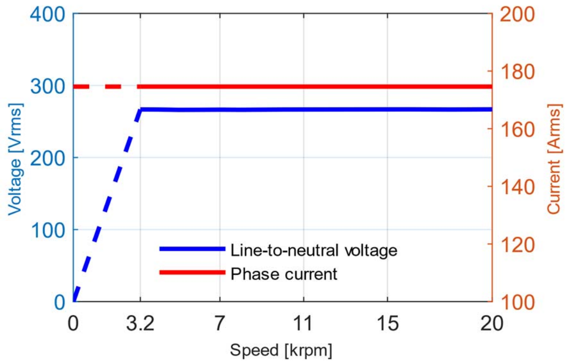

Fig. 10. FEA-based line-to-neutral voltage and phase current vs. speed envelope curves of VSI motor drive

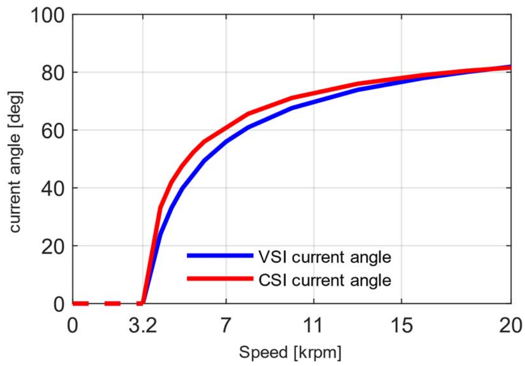

Fig. 11. FEA-based current angle γ between back-emf and phase current for envelope curves of VSI and CSI motor drives

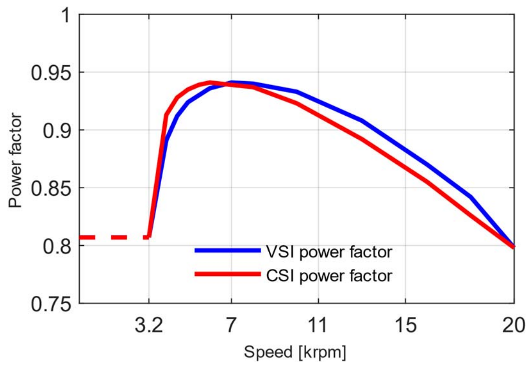

Fig. 12. FEA-based power factor angle θ vs. speed for envelope curves of VSI and CSI motor drives

tips. Due to the different number of winding turns, the CSI-based SPM machine has higher motor output voltage and lower current than the VSI-based SPM machine at the corner speed.

V. Simulation Results

The flux-weakening performance characteristics of the proposed SPM machine with VSI and CSI drives have been evaluated via finite element analysis using JMAG with the following parameters for the CSI: $L_{dc} = 77\ \mu H,\ C = 7.5\ \mu F$. The envelope curves vs. speed for the SPM machine with both CSI and VSI excitation are compared in Fig. 7 and Fig. 8, respectively. Both power curves droop from 100 kW (rated peak power) at the corner point speed of 3,200 rpm to approx. 80 kW at 20 krpm because the machine's characteristic current I_{ch} is approx. 125 % of the rated phase current for peak power operation. If the machine would be redesigned so that I_{ch} is equal to the rated current, the output power at 3,200 rpm and 20 krpm would be nearly equal for both machines.

Fig. 9 and Fig. 10 show the machine line-to-neutral voltage and phase current vs. speed that correspond to the power-torque envelope curves in Fig. 7 (CSI) and Fig. 8 (VSI), respectively. These curves highlight the primary advantage that the CSI offers in comparison with the VSI during flux weakening operation. Since the CSI has the properties of a boost converter, it can readily deliver voltages to the machine terminals that are higher than the dc-link voltage. This means that, for the same delivered power, the higher CSI voltage results in lower required phase current compared to the VSI.

For the machine designs characterized in Table I, the CSI phase current during flux weakening operation is only 123

Arms while the corresponding value for the VSI is 175 Arms, approx. the same ratio as the winding turns ratio in the two machines. As a result, the power cable connecting the CSI and motor is less than half the mass of the corresponding cable for the VSI for the same cable losses [$(123/175)^2 = 0.49$]. In addition to the associated penalty in drive system power density, the larger VSI current will significantly raise the cost of both the cable and connectors compared to those required for the CSI drive. At the other extreme, if the same power cable is used for both inverters, the cable losses for the CSI will be less than half those of the VSI, boosting the drive efficiency.

This difference in current rating also has a similar type of effect on the inverters for the two motor drives since the power switches in the VSI motor drive will be required to handle 42 % higher current than the CSI switches [$(175/123) - 1 = 0.42$]. This will require a larger device die size for the VSI switches to achieve the same conduction losses. Ultimately, the higher VSI current rating is likely to have a negative impact on its mass and volume compared to the CSI since these inverter metrics are typically linked more closely to the inverter's current rating than to its voltage rating.

The inevitable engineering tradeoff associated with this CSI-VSI comparison is that the inverter voltage rating for the CSI will be higher than that of the VSI by the same 42 % ratio noted above for constant power. Depending on the breakpoints in the commercial switch device voltage ratings, the higher voltage requirements of the CSI could raise the cost on this topology, offsetting at least partially the cost penalty suffered by the VSI due to its higher switch current ratings.

For completeness, Fig. 11 and 12 show comparisons of the current angle γ and the power factor, respectively, for the CSI and VSI along the power envelope curves. The fact that they look so similar is expected since the CSI and VSI motors are identical except for the difference in the number of stator winding turns in the two machines.

Before concluding this section, it should be pointed out that wide constant-power speed ratios can be achieved with both the CSI and VSI provided that the machine's characteristic current is properly designed to match the machine's rated current in both cases. However, the CSI is distinguished from the VSI by the fact that it can boost its output terminal voltage while the basic VSI cannot do the same unless a boost dc/dc converter is added at its input. In the absence of this boost converter, the CSI offers a natural advantage over the VSI in the flux weakening regime by making it convenient to lower the current rating of the CSI inverter and power cable, offering benefits for both the CSI drive system cost and power density.

VI. Conclusion

This paper has investigated the impact of the CSI's voltage boost capability on its performance characteristics in the flux weakening regime for a PM machine drive. The *d-q* model of the CSI-based motor including the impact of the ac capacitors is developed to reduce the modeling error in the high-speed regime. The resulting flux weakening performance characteristics of an SPM machine are compared to those of a conventional VSI. It is shown that wide constant-power speed ranges can be achieved with both inverter types with properly designed machines. However, the voltage-boost capability of the CSI makes it possible to reduce its rated current during flux weakening operation compared to that of the VSI. As a result, opportunities are opened to reduce the CSI's inverter and power cable mass compared to the VSI, leading to higher drive system power density and lower cost.

Acknowledgment

This material is based upon work supported by the U.S. Department of Energy's Office of Energy Efficiency and Renewable Energy (EERE) under the Vehicle Technologies Office (VTO), Award Number DE-EE0008704. The authors also gratefully acknowledge the support of the Wisconsin Electric Machines and Power Electronics Consortium (WEMPEC).

References

[1] X. Ding, J. Cheng, and F. Chen, "Impact of Silicon Carbide Devices on the Powertrain Systems in Electric Vehicles," in *Energies,* vol.10, no. 4, pp. 533, April 2017.

[2] X. Ding, H. Guo, R. Xiong, F. Chen, D, Zhang, and C. Gerada, "A New Strategy of Efficiency Enhancement for Traction Systems in Electric Vehicles," in *Applied Energy*, vol. 205, pp. 880-891, Nov. 2017.

[3] L. Junlong, X. Yongxiang, Z. Jibin, W. Baochao, W. Qian, and L. Weiyan, "Analysis and Design of SPM Machines With Fractional Slot Concentrated Windings for a Given Constant Power Region," in IEEE Transactions on Magnetics, vol. 51, no. 11, pp. 1-4, Nov. 2015.

[4] A. M. El-Refaie and T. M. Jahns, "Comparison of synchronous PM machine types for wide constant-power speed range operation," in *Proc. Fourtieth IAS Annual Meeting. Conference Record of the 2005 Industry Applications Conference*, Kowloon, Hong Kong, 2005, pp. 1015-1022.

[5] L. Tang and G. Su, "Boost mode test of a current-source-inverter-fed permanent magnet synchronous motor drive for automotive applications," in *Proc. IEEE 12th Workshop on Control and Modeling for Power Electronics (COMPEL)*, Boulder, CO, 2010, pp. 1-8.

[6] G. Su, L. Tang, and Z. Wu, "Extended constant-torque and constant-power speed range control of permanent magnet machine using a current source inverter," in *Proc. IEEE Vehicle Power and Propulsion Conference*, Dearborn, MI, 2009, pp. 109-115.

[7] H. Dai, T.M. Jahns, R.A. Torres, D. Han, and B. Sarlioglu, "Comparative Evaluation of Conducted Common-Mode EMI in Voltage-Source and Current-Source Inverters using Wide-Bandgap Switches," in *Proc. IEEE Transportation Electrification Conference and Expo (ITEC)*, Long Beach, CA, 2018, pp. 788-794.

[8] M. Hombu, S. Ueda, A. Ueda, and Y. Matsuda, "A new current source GTO inverter with sinusoidal output voltage and current," in *IEEE Trans. on Industry Applications*, vol. 21, no. 5, pp. 1192–1198, Sept./Oct., 1985.

[9] M. Hombu, S. Ueda, and A. Ueda, "A Current Source GTO Inverter with Sinusoidal Inputs and Outputs," in *IEEE Transactions on Industry Applications*, vol. IA-23, no. 2, pp. 247-255, March 1987.

[10] T.M. Jahns and H. Dai, "The past, present, and future of power electronics integration technology in motor drives," in *CPSS Trans. Power Electron. Appl.*, vol. 2, no. 3, pp. 197–216, 2017.

[11] R.A. Torres, H. Dai, W. Lee, T.M. Jahns, and B. Sarlioglu, "Current-Source Inverters for Integrated Motor Drives using Wide-Bandgap Power Switches," in *Proc. IEEE Transportation Electrification Conference and Expo (ITEC)*, Long Beach, CA, 2018, pp. 1002-1008.

[12] L. Tang and G. Su, "Boost mode test of a current-source-inverter-fed permanent magnet synchronous motor drive for automotive applications," in *Proc. IEEE 12th Workshop on Control and Modeling for Power Electronics (COMPEL)*, Boulder, CO, 2010, pp. 1-8.

[13] Z. Wu and G. Su, "High-performance permanent magnet machine drive for electric vehicle applications using a current source inverter," in *Proc. 34th Annual Conference of IEEE Industrial Electronics*, Orlando, FL, 2008, pp. 2812-2817.